Publ. Astron. Soc. Jpn 2014 66 (2), 38 (1–7)
doi: 10.1093/pasj/psu003
Advance Access Publication Date: 2014 April 16

Accurate parallax measurement toward the symbiotic star R Aquarii

Cheulhong Min,[1,2,*] Naoko Matsumoto,[2] Mi Kyoung Kim,[3] Tomoya Hirota,[1,2] Katsunori M. Shibata,[1,2] Se-Hyung Cho,[3] Makoto Shizugami,[2] and Mareki Honma[1,2]

[1]Department of Astronomical Sciences, The Graduate University for Advanced Studies, 2-21-1 Osawa, Mitaka, Tokyo 181-8588
[2]Mizusawa VLBI Observatory, National Astronomical Observatory of Japan, 2-21-1 Osawa, Mitaka, Tokyo 181-8588
[3]Korea Astronomy and Space Science Institute, 776 Daedukdaero (61-1 Whaam), Yuseong, Daejeon 305-348, Korea

*E-mail: cheulhong.min@nao.ac.jp

Received 2013 September 24; Accepted 2013 November 23

Abstract

Multiepoch phase-referencing VLBI (Very Long Baseline Interferometry) observations with VERA (VLBI Exploration of Radio Astrometry) were performed for the symbiotic star R Aquarii (R Aqr) from 2005 September to 2006 October. Tracing one of the $v = 2$, $J = 1$–0 SiO maser spots, we measured an annual parallax of $\pi = 4.59 \pm 0.24$ mas, corresponding to a distance of 218^{+12}_{-11} pc. Our result is consistent with earlier distance measurements, but yields the highest accuracy of $\sim$5% level. Applying our distance, we derived an absolute K-band magnitude of $M_K = -7.71 \pm 0.11$, which is consistent with the recent period–luminosity relation by VLBI parallax measurements for five OH-Mira variables. In addition, the expansion age of an inner nebula around R Aqr is found to be $\sim$240 yr, corresponding to about the year 1773.

Key words: astrometry — binaries: symbiotic — instrumentation: interferometers — masers (SiO) — stars: individual (R Aquarii)

1 Introduction

The class of "symbiotic star" was first introduced by Merrill (1958), who presented the characteristic spectrum showing a combination of the giant star continuum with molecular absorption features and ionized emission lines. These stars are nowadays generally understood as interacting binary systems comprising a cool late-type star, which is a red giant (RG) or asymptotic giant branch (AGB) star, and a hot compact companion, usually a white dwarf or in a few cases a low-mass main-sequence star. Phenomena caused by interaction between the components in symbiotic stars, such as accretions of the stellar material around the hot component with novalike thermonuclear outbursts, mass loss from a giant star with colliding wind process, formation of bipolar photoionized planetary nebulae, and collimation of a jet-like feature, provide unique astrophysical laboratories to investigate the evolution of binary systems (Kenyon 1986).

R Aquarii (R Aqr) is one of the most studied symbiotic stars composed of a Mira, a long period variable, with a pulsation period of $\sim$387 d and a putative white dwarf companion as well as ionized nebulae around the system. Unusually, R Aqr exhibits an astronomical jet feature that

is probably powered by an accretion disk around a white dwarf companion. This jet has been extensively observed in optical, radio, UV, and X-ray wavelengths and is known to extend up to $\sim$2500 au in a NE–SW direction with a shock speed of $\sim$235–285 km s^{-1} (Nichols & Slavin 2009).

Large-scale extended inner and outer nebulae are also known in R Aqr. Solf and Ulrich (1985) carried out an extensive study of the nebulae using optical spectroscopic observations, and revealed that both nebulae had the same geometric structure resembling a bipolar, hourglasslike shape extending $\sim 2'$ in an east–west direction for the outer nebula with an equatorial velocity of 55 km s^{-1} and $\sim 1'$ in a north–south direction for the inner nebula with an equatorial velocity of 32 km s^{-1}.

An orbital period of 44 yr for R Aqr was proposed by Willson, Garnavich, and Mattei (1981), who interpreted the depressions of the optical light curve from 1928 to 1934 and from 1974 to 1978 as attributed to the obscuration of the Mira variable by an extended cloud of dust. Radial velocity data covering a wide range were collected by McIntosh and Rustan (2007) in visual, near-IR, and radio wavelengths from 1940. They extracted an orbital period of 34.6 yr with an eccentricity of 0.52, and a projected semimajor axis of 3.5 au. Subsequently, Gromadzki and Mikołajewska (2009) also extracted an orbital period of 43.6 yr with an eccentricity of 0.25, modifying the radial velocity data collected by McIntosh and Rustan (2007) complemented by additional radial velocity data. They obtained an orbital period consistent with Willson, Garnavich, and Mattei (1981).

In addition, R Aqr is one of three symbiotic stars that have circumstellar masers associated with Mira variables. Since the first detection of an SiO maser toward R Aqr by Lépine, Le Squeren, and Scales (1978), there have been several single-dish observational studies of 43/86/128 GHz SiO masers (Zuckerman 1979; Cohen & Ghigo 1980; Spencer et al. 1981; Martínez et al. 1988; Jewell et al. 1991; Schwarz et al. 1995; Cho et al. 1996; Alcolea et al. 1999; Pardo et al. 2004; Kang et al. 2006) as well as 22/321 GHz H_2O masers (Seaquist et al. 1995; Ivison et al. 1994, 1998). Moreover, high-resolution Very Long Baseline Interferometry (VLBI) observations were also performed with VLBA, presenting a ringlike structure of the 43 GHz SiO maser with an approximated diameter of 30 mas (Boboltz et al. 1997; Hollis et al. 2001; Cotton et al. 2004, 2006).

VLBI monitor observations of SiO masers toward R Aqr were carried out since 2004 by Kamohara et al. (2010) with VERA. They observed both $v = 1$ and $v = 2$, $J = 1$–0 SiO maser transitions, and confirmed that both maser emissions appear in similar regions. However, each transition of maser spots was not exactly coincident with the other within a range of spatial and spectral resolutions, so that new theoretical studies were required for looking into the finer details of both maser distributions in the inner shells around the central AGB star. They also estimated an annual parallax of 4.7 $\pm$ 0.8 mas assuming that the position of the star is coincident with the center of circular fitting of both SiO maser distributions, because of the short lifetime of individual SiO maser spots.

A typical lifetime of an SiO maser feature is of the order of 100 d, but a few cases of the SiO maser features persist for a period of 1 yr. The best example is high-resolution VLBA monitoring observations for the SiO maser in the Mira variable of TX Cam (Diamond & Kemball 1999, 2003; Gonidakis et al. 2010). According to the results by Diamond and Kemball (2003) and Gonidakis, Diamond, and Kemball (2010), the lifetime of the SiO maser components around the Mira variable was suggested to be between 150 and 200 d, but sometimes long-lived maser components persisted over 350 d. Moreover, McIntosh and Bonde (2010) reported that the average lifetime of the SiO maser features was 171 d, but also reported the existence of long-lived SiO maser features over 171 d.

The VERA array of the National Astronomical Observatory of Japan (NAOJ) is a Japanese VLBI array aimed at obtaining 10-microarcsecond-level accuracy of parallaxes and proper motions of H_2O, SiO, and CH_3OH maser sources by using its unique dual-beam phase-referencing technique. In past years, VERA has successfully measured parallaxes for maser sources in our Galaxy, including AGB stars, such as S Crt (Nakagawa et al. 2008), SY Scl (Nyu et al. 2011), and RX Boo (Kamezaki et al. 2012). Accurate measurements of distances for AGB stars would be useful for calibrating the period–luminosity relation precisely, which provides a fundamental basis for a distance ladder of nearby galaxies.

In this paper, we report on phase-referencing observations of the SiO maser toward the symbiotic star R Aqr using VERA, and present the result of the most accurate parallax measurement.

2 Observations and data reduction

The observations of the $v = 1$ and $v = 2$, $J = 1$–0 SiO maser transitions were performed by using the four stations of VERA from 2005 September to 2006 October. We reanalyzed these data, which were published by Kamohara et al. (2010). Rest frequencies of 43.122079 GHz and 42.820582 GHz were adopted in this paper for the $v = 1$, $J = 1$–0 and $v = 2$, $J = 1$–0 transitions, respectively.

The target source of the SiO masers around R Aqr ($\alpha_{J2000.0} = 23^h43^m49^s.4616$, $\delta_{J2000.0} = -15^\circ17'04''.202$) and the phase-referencing source J2348−1631 ($\alpha_{J2000.0} = 23^h48^m02^s.608532$, $\delta_{J2000.0} = -16^\circ31'12''.02226$) were observed simultaneously with the VERA dual-beam system. The separation angle between the target and reference source is $\sim 1^\circ.6$. A bright continuum source, 3C 454.3, was also observed every 80 min as a calibrator. The instrumental phase difference between the two beams was measured in real time during the observations by correlating random signals from artificial noise sources injected into both beams at each station (Honma et al. 2008).

The data were recorded onto magnetic tapes at a rate of 1024 Mbps with the VERA DIR2000 recording system, providing a total bandwidth of 256 MHz with 2-bit digitization. The 256 MHz bandwidth data were divided into 16 IF channels (16 MHz each), and two of them were assigned to the $v = 1$ and $v = 2$, $J = 1$–0 SiO maser transitions of the target source, while others were assigned to the continuum spectrum of the reference and the calibrator source. Correlation processing was carried out on the Mitaka FX correlator located in NAOJ, Mitaka. The spectral resolution of the maser lines was set to be 31.25 kHz, corresponding to a velocity resolution of 0.21 km s^{-1} for observation epochs of 2005/270, 2006/207, 242, 286 (year/day of year), and 15.625 kHz, corresponding to a velocity resolution of 0.11 km s^{-1} for 2005/327, 358, 2006/045, 062, 128.

All the data reductions were performed by using the National Radio Astronomy Observatory (NRAO) Astronomical Image Processing System (AIPS). The amplitude and the bandpass calibrations for the target source and the reference source were made independently. For phase-referencing analysis, we calibrated the clock parameters using the calibrator, 3C 454.3, and the fringe fitting was made on the position reference source, J2348−1631, to obtain the residual fringe phase. These solutions were applied to the target source, R Aqr. The dual-beam phase-calibration data and the modified delay-tracking model were also applied to the target data in order to obtain accurate astrometry with VERA. Then, using AIPS task IMAGR, we obtained the $v = 1$ and $v = 2$ maser images which consist of 2048 × 2048 pixels with a pixel spacing of 0.05 mas. From these images, we searched for maser spots with S/N ratio larger than six against the detection criterion, and measured their positions by elliptical Gaussian fitting using the AIPS task SAD. Selected maser spots were considered to be real if maser spots existed in more than two adjacent channel maps within the beam size.

3 Parallax measurement

In order to estimate a parallax, we assumed that the motion of the SiO maser spot is the summation of a parallax motion and a linear proper motion. The linear proper motion includes an individual motion of the maser spot in the maser-emitting region and a secular motion of the central star, as well as a binary motion. However, an accelerating or decelerating factor of the binary motion is negligible and considered to be linear for one year of a 44 yr orbit. Then, the motion of the maser spot on the sky plane is simply described by the following equations (Seidelmann 1992):

$$\alpha(t)\cos\delta = \alpha_0 + \mu_\alpha^*(t - t_0) + \pi P_\alpha,$$
$$\delta(t) = \delta_0 + \mu_\delta(t - t_0) + \pi P_\delta, \quad (1)$$

where (α_0, δ_0) are the initial positions at $t = t_0$, $(\mu_\alpha^*, \mu_\delta)$ are the linear proper motions for the direction of right ascension and declination (note that $\mu_\alpha^* = \mu_\alpha \cos\delta$), π is the parallax, (P_α, P_δ) are the parallax factors, which are sinusoidal functions of the parallactic ellipse for a certain time in right ascension and declination due to the motion of the Earth around the Sun. The parallax factors are computed as follows:

$$P_\alpha = X_\odot \sin\alpha_\star - Y_\odot \cos\alpha_\star,$$
$$P_\delta = X_\odot \cos\alpha_\star \sin\delta_\star + Y_\odot \sin\alpha_\star \sin\delta_\star - Z_\odot \cos\delta_\star, \quad (2)$$

where $(X_\odot, Y_\odot, Z_\odot)$ are the Cartesian coordinates of the Earth relative to the barycenter of the solar system at the time of observation. These values are taken from the NASA Jet Propulsion Laboratory Solar System ephemeris (e.g., DE405). $(\alpha_\star, \delta_\star)$ are the position of the target (the nominal position) in right ascension and declination, respectively.

Unknown parameters, parallax (π), linear proper motions $(\mu_\alpha^*, \mu_\delta)$, and initial positions (α_0, δ_0) were fitted independently with respect to right ascension and declination directions by reduced χ^2 fittings. The astrometric position errors were set so that the reduced χ^2 becomes unity. Then, combined fit with both directions was conducted by giving uniform weights of σ_{RA} and σ_{Dec} in right ascension and declination, respectively.

Among all the observations, we used an SiO maser ($v = 2$, $J = 1$–0) spot with $V_{LSR} = -20.7$ km s^{-1} to estimate parallax. Figure 1 shows the phase-referenced image of the target maser spot, and this spot was found to be persistent. We detected this spot in eight epochs at 2005/270, 327, 358, 2006/045, 062, 128, 207, and 286, covering a period of ~ 1 yr in the same velocity channel. In figure 2, we present position variations of the traced

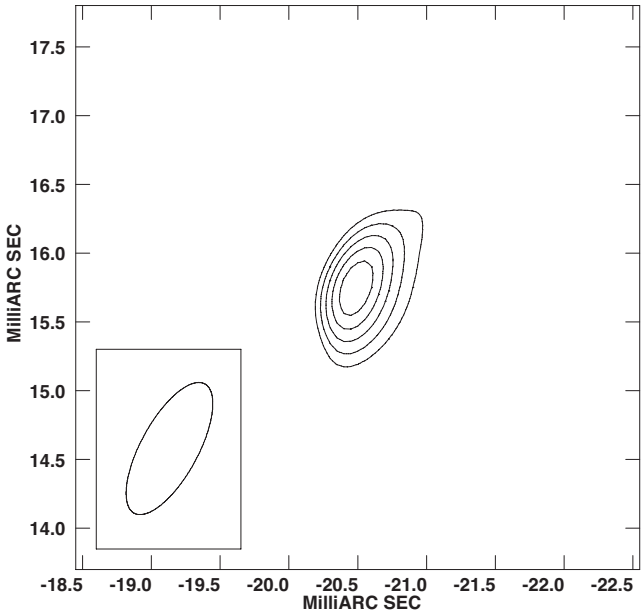

Fig. 1. Phase-referenced image of the $v = 2$, $J = 1$–0 ($V_{\rm LSR} = -20.7\,{\rm km\,s^{-1}}$) SiO maser spot at the first epoch on 2005/270. The x and y axes represent the RA and Dec offset with respect to the center coordinates of $(\alpha, \delta)_{\rm J2000.0} = (23^{\rm h}43^{\rm m}49\overset{\rm s}{.}4736, -15^\circ17'4\overset{''}{.}3620)$. The peak intensity is 1.77 Jy beam^{-1}, and contour levels are set to 7, 9, 11, 13, and 15σ, where σ is the rms noise of 0.11 Jy beam^{-1}. The synthesized beam is 1.07 mas $\times$ 0.42 mas (PA $= -29^\circ$) and is shown in the bottom-left corner of the figure.

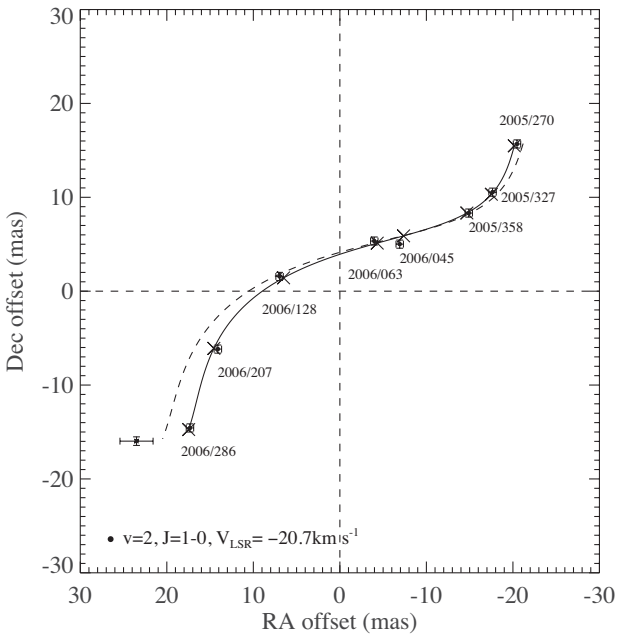

Fig. 2. Measured positions of the $v = 2$, $J = 1$–0 ($V_{\rm LSR} = -20.7\,{\rm km\,s^{-1}}$) SiO maser spots. The solid line indicates the best-fitting result of parallax and proper motion. The center coordinates are $(\alpha, \delta)_{\rm J2000.0} = (23^{\rm h}43^{\rm m}49\overset{\rm s}{.}4736, -15^\circ17'4\overset{''}{.}3620)$. The filled circles with error bars of $\sigma_{\rm RA} = 0.430$ mas and $\sigma_{\rm Dec} = 0.434$ mas in RA and Dec directions (see text) indicate the positions of the traced maser spot, and cross symbols represent the predicted positions. The dashed line and the asterisk symbol with error bar indicate the misidentified case (see text).

SiO maser spot with the best-fitting parallax and proper motion results presented by the solid curve. Table 1 shows a summary of the parallax and the linear proper motion results with uniform weights in right ascension and declination. By setting the position errors of $\sigma_{\rm RA} = 0.430$ mas and $\sigma_{\rm Dec} = 0.434$ mas obtained by reduced χ^2 fitting, we obtained the parallax of $\pi = 4.59 \pm 0.24$ mas, corresponding to a distance of 218^{+12}_{-11} pc. The proper motions are also obtained to be $\mu^*_\alpha = 37.13 \pm 0.47\,{\rm mas\,yr^{-1}}$ and $\mu_\delta = -28.62 \pm 0.44\,{\rm mas\,yr^{-1}}$, respectively.

Note that we detected another maser spot other than the target maser spot in the velocity channel with $V_{\rm LSR} = -20.7\,{\rm km\,s^{-1}}$ on the observation epochs of 2005/358 and 2006/286. Two maser spots were closely located within 0.51 mas on 2005/358, but separated by $\sim$6.33 mas on 2006/286. To avoid misidentification of the target maser spot, we tried estimating parallax with each maser spot. For the maser spots on 2005/358, measured parallaxes for individual cases practically presented the same result. On the other hand, the fitting result was significantly worse for 2006/286 when we misidentified one of the maser spots detected on this epoch, as shown in figure 2. Thus, we concluded that the two maser spots on 2006/286 fall into two distinct maser features, and the worse-fitting maser spot is excluded for parallax measurement.

4 Discussions

4.1 Distance toward R Aqr

Previously, distance measurements toward R Aqr had mostly been done by using three methods: (1) the kinematic method using the nebulae around the system, (2) the period–luminosity method, and (3) direct distance measurement by parallax. We summarize the distance measurements toward R Aqr in table 2, including the result of the present study.

The first kinematic distance measurement toward R Aqr was introduced by Baade (1943, 1944). He deduced a distance of 260 pc based on a constant expansion velocity for the outer nebula of between 80 and 100 km s^{-1} with an expansion age of $\sim$600 yr. In addition, Solf and Ulrich (1985) described the two nebulae as having dense equatorial ring structures with equatorial expansion velocities of 32 and 55 km s^{-1} for the inner and outer nebulae, respectively. By adopting the expansion age for the outer nebula of 600 yr and the inner nebula of 180 yr from Baade (1944) and Sopka et al. (1982) respectively, they deduced the distance of 180 pc and 185 pc for the outer and the inner nebula respectively. Recently, Korean historical records provided two irregular outbursts called "Guest Star" epochs in AD 1073 and 1074 (Yang et al. 2005). Based on the records,

Table 1. Parallax and linear proper motion fitting result.

V_{LSR} (km s^{-1})	π (mas)	Distance (pc)	μ_α^* (mas yr^{-1})	μ_δ (mas yr^{-1})	σ (mas)
−20.7	4.65 ± 0.29	215^{+15}_{-13}	37.08 ± 0.53	—	0.430
	4.38 ± 0.53	228^{+32}_{-25}	—	-28.56 ± 0.49	0.434
	4.59 ± 0.24	218^{+12}_{-11}	37.13 ± 0.47	-28.62 ± 0.44	—

Table 2. Historical distance measurements toward R Aqr.

	Distance	Method
Baade (1943)	260 pc	outer nebula kinematic
Solf and Ulrich (1985)	180 pc	outer nebula kinematic
Solf and Ulrich (1985)	185 pc	inner nebula kinematic
Yang et al. (2005)	273 pc	outer nebula kinematic
Whitelock, Feast, and and van Leeuwen (2008)	250 pc	period–luminosity relation
ESA (1997)	197^{+323}_{-75} pc	Hipparcos parallax
Kamohara et al. (2010)	214^{+45}_{-32} pc	VERA parallax
Our result	218^{+12}_{-11} pc	VERA parallax

they estimated a kinematic distance of ∼273 pc with a constant expansion velocity of 55 km s^{-1} from Solf and Ulrich (1985).

In pulsating stars, one noticeable and useful property is the period–luminosity relation. This relation has been an important indicator of distances toward pulsating stars.

Recent period–luminosity relations in AGB stars were provided by Whitelock, Feast, and van Leeuwen (2008), who reanalyzed the revised Hipparcos parallaxes and compared them with VLBI parallax measurements. They established the period–luminosity relation in the infrared K-band magnitude:

$$M_K = \rho(\log P - 2.38) + \delta, \quad (3)$$

where they obtained a slope of $\rho = -3.51 \pm 0.20$ and a zero point of $\delta = -7.25 \pm 0.05$ for the O-rich Mira variables in our Galaxy. Using their period–luminosity relation, Whitelock, Feast, and van Leeuwen (2008) presented a distance of 250 pc for R Aqr.

According to Hipparcos observations (ESA 1997), the parallax of R Aqr was 5.07 ± 3.15 mas, which corresponds to a distance of 197^{+323}_{-75} pc. More accurate parallax measurement was achieved by Kamohara et al. (2010) using the SiO maser distributions around the Mira variable in R Aqr with VERA observations. They followed the center of circular ring fitting of the SiO maser distributions, and yielded an annual parallax of $\pi = 4.7 \pm 0.8$ mas, corresponding to a distance of 214^{+45}_{-32} pc.

Our parallax measurement of $\pi = 4.59 \pm 0.24$ mas ($D = 218^{+12}_{-11}$ pc) is consistent with previous parallax measurement results, but yields the distance with the highest accuracy level of ∼5%. Compared with the distance measurements from other methods, our result is smaller than the distance obtained by the period–luminosity relation. According to the period–luminosity relation by Whitelock, Feast, and van Leeuwen (2008), the expected absolute K-band magnitude for R Aqr is $M_K = -7.98 \pm 0.09$, with a pulsation period of 387 d. Adopting an apparent K-band magnitude of $m_K = -1.02$ obtained from SAAO (South African Astronomical Observatory) by Whitelock, Marang, and Feast (2000), our distance measurement provides the absolute magnitude of $M_K = -7.71 \pm 0.11$. Although this value does not include the error in apparent K-band magnitude, our distance result presents a lower K-band absolute magnitude than that provided by the period–luminosity relation in Whitelock, Feast, and van Leeuwen (2008). On the other hand, Whitelock, Feast, and van Leeuwen (2008) also showed that the period–luminosity relation estimated by only VLBI parallaxes of 5 OH-Mira provides a zero point of $\delta = -7.08 \pm 0.17$. This relation yields the absolute K-band magnitude of $M_K = -7.82 \pm 0.16$, which is consistent with our result. However, more VLBI parallax measurements are needed to establish a reliable period–luminosity relation in the future, since there are only five VLBI parallax measurements for Mira variables in their relation.

Moreover, kinematic distances for R Aqr have a large range from 180 to 270 pc based on the nebula properties such as angular size, expansion age, and expansion velocity of the nebula. In the case of the inner nebula, kinematic properties with the equatorial shell radius of 6.″5 and the equatorial expansion velocity of 32 km s^{-1} were derived using a kinematic model from Solf and Ulrich (1985). Applying our distance to their properties, the equatorial shell radius for the inner nebula corresponds to the scale of 1494^{+78}_{-70} au. We assumed that the inner nebula has a constant expansion rate with the velocity from Solf and Ulrich (1985), and then estimated that the expansion age of the inner nebula is ∼240 yr, corresponding to about the year 1773.

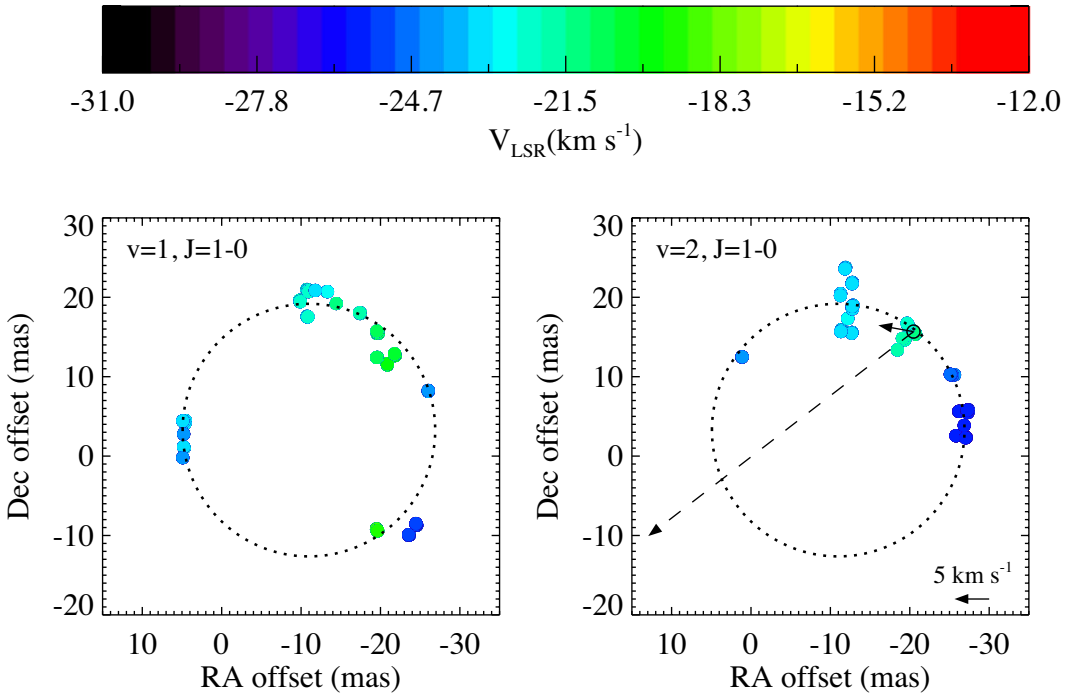

Fig. 3. Distribution of phase-referencing SiO maser spots toward R Aqr and fitted circle from both maser transitions at 2005/270. Left: SiO $v = 1$, $J = 1$–0 maser transition distribution. Right: SiO $v = 2$, $J = 1$–0 maser transition distribution. The center coordinates are $(\alpha, \delta)_{J2000.0} = (23^{h}43^{m}49^{s}.4736, -15^{\circ}17'4''.3620)$. The top color bar denotes the LSR velocity range of -12 to $-31\,\mathrm{km\,s^{-1}}$. The open black circle symbol indicates the maser spot for parallax measurement. The dashed arrow indicates the linear proper motion of the traced maser spot, and the solid arrow indicates the subtracted proper motion from the motion of the central star from Kamohara et al. (2010). The dotted circle presents the circular fitting of both SiO transitions with a radius of 15.90 mas. (Color online)

On the other hand, the outer nebula is suggested to have been formed in AD 1073 and 1074 from the outburst record found by Yang et al. (2005). Recently, a nitrate ion recorded in the Antarctic ice core also supported a nova eruption of R Aqr between AD 1060 and 1080 (Tanabe & Motizuki 2012). In the case of the outer nebula, kinematic properties with the equatorial shell radius of 42″ and the expansion velocity of $55\,\mathrm{km\,s^{-1}}$ were also reported by Solf and Ulrich (1985). The outburst record with our distance measurement suggested that the assumed constant expansion velocity for the outer nebula is $\sim 48 \pm 2\,\mathrm{km\,s^{-1}}$ with an angular size of 42″. This suggests that the expansion velocity of the outer nebula might be smaller than $55\,\mathrm{km\,s^{-1}}$, or the expansion of the outer nebula might be accelerated.

4.2 Proper motion of the maser spot

Along with the parallax measurement, tracing the maser spot also presents the linear proper motion of $\mu_\alpha^* = 37.13 \pm 0.47\,\mathrm{mas\,yr^{-1}}$ and $\mu_\delta = -28.62 \pm 0.44\,\mathrm{mas\,yr^{-1}}$ in right ascension and declination, respectively. By converting to a physical scale, the proper motion of the maser spot is equivalent to $\sim 48.45\,\mathrm{km\,s^{-1}}$ in a south-easterly direction (1 mas $\mathrm{yr^{-1}}$ corresponds to $1.03\,\mathrm{km\,s^{-1}}$ at the distance of 218 pc).

According to the result from Kamohara et al. (2010), the linear proper motion of R Aqr was $\mu_\alpha^* = 32.2 \pm 0.8\,\mathrm{mas\,yr^{-1}}$ and $\mu_\delta = -29.5 \pm 0.7\,\mathrm{mas\,yr^{-1}}$, which includes the secular motion and the binary motion of the central star. Our linear proper motion of the maser spot is also composed of the secular motion and the binary motion as well as the individual motion of the maser spot, so that the subtracted proper motion vector from the result of Kamohara et al. (2010) indicates the internal individual motion of the maser spot in the maser-emitting region. The subtracted motion of the maser spot with respect to the motion of the central star is $4.93 \pm 1.27\,\mathrm{mas\,yr^{-1}}$ and $0.88 \pm 1.14\,\mathrm{mas\,yr^{-1}}$ in right ascension and declination respectively. The magnitude of the proper motion is $\sim 5.17\,\mathrm{km\,s^{-1}}$ in an easterly direction with a position angle of $\sim 280^{\circ}$.

The distributions obtained from the $v = 1$ and $v = 2$, $J =$ 1–0 SiO maser spots and proper motion vectors are displayed in figure 3. We also present the result of circular fitting to both transitions of SiO maser spots in figure 3. In the maser distributions, the traced maser spot, denoted by a black circle in figure 3, is likely to show a motion along the maser-emitting shell that corresponds to the circle of the SiO maser distribution. The overall motion of the SiO maser shell was suggested to be contracting by

Kamohara et al. (2010), who estimated an infall velocity of $3.1 \pm 0.6\,\mathrm{km\,s^{-1}}$. However, in our result, the proper motion of the traced maser spot does not seem to have any inward motion. Although overall motions of maser features have a radial motion of expansion or contraction following the motion of the SiO maser-emitting region in the circumstellar envelope, some cases of maser components appear to move arbitrarily due to the complex dynamics of the circumstellar SiO maser shell.

In the previous VLBI observations by Boboltz, Diamond, and Kemball (1997), they also provided an average inward motion of individual maser components with a mean infall speed of $4.2 \pm 0.9\,\mathrm{km\,s^{-1}}$. However, some of the components appeared to move arbitrarily with respect to inward motion. Individual SiO maser components in TX Cam also presented complex motions not only in the plane of the sky, but also along the line of sight. These motions are thought to be attributable to turbulence in the maser shell, and also to changes in the conditions conducive to maser emission (Gonidakis et al. 2010).

A rotating SiO maser shell proposed by Hollis et al. (2000, 2001) was also a proposal considered for our proper motion result. However, the velocity gradients of the SiO maser distributions were inconsistent with Hollis et al. (2001), and no observation epochs were compatible with the rotating maser shell.

Acknowledgments

We would like to thank all the VERA staff members for their assistance concerning the array operations and data correlations. This work was supported in part by The Graduate University for Advanced Studies (Sokendai).

References

Alcolea, J., et al. 1999, A&AS, 139, 461
Baade, W. A. 1943, Annual Report of the Director of the Mount Wilson Observatory 1942–1943 (Washington, DC: Carnegie Institution), 17
Baade, W. A. 1944, Annual Report of the Director of the Mount Wilson Observatory 1943–1944 (Washington, DC: Carnegie Institution), 12
Boboltz, D. A., Diamond, P. J., & Kemball, A. J. 1997, ApJ, 487, L147
Cho, S.-H., Kaifu, N., & Ukita, N. 1996, A&AS, 115, 117
Cohen, N. L., & Ghigo, F. D. 1980, AJ, 85, 451
Cotton, W. D., et al. 2004, A&A, 414, 275
Cotton, W. D., et al. 2006, A&A, 456, 339
Diamond, P. J., & Kemball, A. J. 1999, in IAU Symp. 191, Asymptotic Giant Branch Stars, ed. T. Le Bertre et al. (San Francisco: ASP), 195
Diamond, P. J., & Kemball, A. J. 2003, ApJ, 599, 1372
Diamond, P. J., Kemball, A. J., Junor, W., Zensus, A., Benson, J., & Dhawan, V. 1994, ApJ, 430, L61
ESA 1997, The Hipparcos and Tycho Catalogues, ESA SP-1200 (Noordwijki: ESA)
Gonidakis, I., Diamond, P. J., & Kemball, A. J. 2010, MNRAS, 406, 395
Gromadzki, M., & Mikołajewska, J. 2009, A&A, 495, 931
Hollis, J. M., Boboltz, D. A., Pedelty, J. A., White, S. M., & Forster, J. R. 2001, ApJ, 559, L37
Hollis, J. M., Pedelty, J. A., Forster, J. R., White, S. M., Boboltz, D. A., & Alcolea, J. 2000, ApJ, 543, L81
Honma, M., et al. 2008, PASJ, 60, 935
Ivison, R. J., Seaquist, E. R., & Hall, P. J. 1994, MNRAS, 269, 218
Ivison, R. J., Yates, J. A., & Hall, P. J. 1998, MNRAS, 295, 813
Jewell, P. R., Snyder, L. E., Walmsley, C. M., Wilson, T. L., & Gensheimer, P. D. 1991, A&A, 242, 211
Kamezaki, T., et al. 2012, PASJ, 64, 7
Kamohara, R., et al. 2010, A&A, 510, A69
Kang, J., Cho, S.-H., Kim, H.-G., Chung, H.-S., Kim, H.-R., Roh, D.-G., Lee, C.-W., & Kim, S.-J. 2006, ApJS, 165, 360
Kenyon, S. J. 1986, The Symbiotic Stars (Cambridge: Cambridge University Press)
Lépine, J. R. D., Le Squeren, A. M., & Scales, E., Jr. 1978, ApJ, 225, 869
Martínez, A., Bujarrabal, V., & Alcolea, J. 1988, A&AS, 74, 273
McIntosh, G. C., & Bonde, J. 2010, PASP, 122, 396
McIntosh, G. C., & Rustan, G. 2007, AJ, 134, 2113
Merrill, P. W. 1958, Etoiles á Raies d'Emission (Cointe-Sclessin: Institut d'Astrophysique), 20, 436
Nakagawa, A., et al. 2008, PASJ, 60, 1013
Nichols, J., & Slavin, J. D. 2009, ApJ, 699, 902
Nyu, D., et al. 2011, PASJ, 63, 63
Pardo, J. R., Alcolea, J., Bujarrabal, V., Colomer, F., del Romero, A., & de Vicente, P. 2004, A&A, 424, 145
Schwarz, H. E., Nyman, L.-Å., Seaquist, E. R., & Ivison, R. J. 1995, A&A, 303, 833
Seaquist, E. R., Ivison, R. J., & Hall, P. J. 1995, MNRAS, 276, 867
Seidelmann, P. K. 1992, Explanatory Supplement to the Astronomical Almanac (Mill Valley, CA: University Science Books), 121
Solf, J., & Ulrich, H. 1985, A&A, 148, 274
Sopka, R. J., Herbig, G., Kafatos, M., & Michalitsianos, A. G. 1982, ApJ, 258, L35
Spencer, J. H., Winnberg, A., Olnon, F. M., Schwartz, P. R., Matthews, H. E., & Downes, D. 1981, AJ, 86, 392
Tanabe, K., & Motizuki, Y. 2012, Mem. Soc. Astron. Ital., 83, 840
Whitelock, P. A., Feast, M. W., & van Leeuwen, F. 2008, MNRAS, 386, 313
Whitelock, P., Marang, F., & Feast, M. W. 2000, MNRAS, 319, 728
Willson, L. A., Garnavich, P., & Mattei, J. A. 1981, IBVS, 1961
Yang, H.-J., Park, M.-G., Cho, S.-H., & Park, C. 2005, A&A, 435, 207
Zuckerman, B. 1979, ApJ, 230, 442